

Early detection of impact fatigue damage in an adhesively-bonded connection using acoustic emission

Khoshmanesh, S.; Watson, S. J.; Zarouchas, D.

DOI

[10.1016/j.engstruct.2024.117973](https://doi.org/10.1016/j.engstruct.2024.117973)

Publication date

2024

Document Version

Final published version

Published in

Engineering Structures

Citation (APA)

Khoshmanesh, S., Watson, S. J., & Zarouchas, D. (2024). Early detection of impact fatigue damage in an adhesively-bonded connection using acoustic emission. *Engineering Structures*, 308, Article 117973. <https://doi.org/10.1016/j.engstruct.2024.117973>

Important note

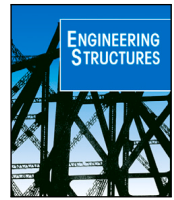
To cite this publication, please use the final published version (if applicable). Please check the document version above.

Copyright

Other than for strictly personal use, it is not permitted to download, forward or distribute the text or part of it, without the consent of the author(s) and/or copyright holder(s), unless the work is under an open content license such as Creative Commons.

Takedown policy

Please contact us and provide details if you believe this document breaches copyrights. We will remove access to the work immediately and investigate your claim.



Early detection of impact fatigue damage in an adhesively-bonded connection using acoustic emission

S. Khoshmanesh^{*}, S.J. Watson, D. Zarouchas

Faculty of Aerospace Engineering, TU Delft, Kluyverweg 1, 2629 HS Delft, The Netherlands

ARTICLE INFO

Keywords:

Adhesive joint
Impact
Fatigue
Damage detection
Acoustic emission

ABSTRACT

Wind turbine blades carry the risk of impact damage during transportation, installation, and operation. Such impacts can cause levels of damage that can propagate throughout the structure compromising performance and safety. In this study, the effect of impact damage on fatigue damage propagation in test specimens representative of a spar cap-shear web adhesively-bonded connection of a wind turbine blade was investigated. In addition, the effectiveness of using acoustic emissions to detect early impact-induced fatigue damage was studied. Three impact tests with increasing levels of energy were investigated. The results showed that for an impact test with an average energy of 16.32 J, the fatigue damage accumulation process was not influenced by the size and location of the impact damage. But for impact tests with an average energy of 23.68 J and 32.13 J, greater crack density and accelerated de-lamination and de-bonding of the adhesive from the laminate could be seen in the impact zone. Acoustic emission was shown to identify the position of the damage zone for the higher energy impact tests. It was also effective in showing the progressive accumulation of fatigue damage in this zone during the fatigue test.

1. Introduction

With the increasing size of wind turbine blades, transportation, and installation, especially offshore become ever more challenging. Installation is usually carried out by floating crane vessels. These vessels are subject to the wave-induced motion which leads to the movement of the crane tip and the possibility of blade strikes on the hub or tower [1]. It is prudent to consider this risk and to evaluate the effect of an impact load on a blade.

A wind turbine blade consists of aerodynamic composite shells (facing the pressure side and suction side) and shear webs which are molded separately and then bonded together in an assembly process using a structural adhesive. The load-carrying parts of the shells (spar caps) are constructed from uni-directional composite laminates such as thick GFRM (glass fiber-reinforced materials) [2–4]. This spar cap-shear web adhesively-bonded connection is a key element for the structural integrity of the blade. Impacts can induce damage in this structure and affect the overall integrity of the blade structure. During the lifetime of a wind turbine, blades need to be periodically inspected. In this study, an evaluation is made of the measurement of structure-borne acoustic emissions and how they could assist in the health monitoring of a blade especially to detect fatigue damage resulting from earlier impacts.

Chou et al. investigated the inception of failure in carbon fiber reinforced composite (CFRP) pressure vessels by measuring the accumulation of AE events during a pressure test [5]. It was concluded that

an abrupt increase in the AE hit rate is an indication of the initiation of failure of the vessel. Lissek et al. tried to correlate the crack growth during the inter-laminar toughness testing of a fiber-reinforced composite material to the material properties. They used a double cantilever beam (DCB) test specimen and measured the cumulative energy of AE events during a quasi-static loading process and observed a jump in the cumulative energy during the loading process which was taken as a sign of the initiation of damage [6]. Nikbakht et al. studied the delamination of a composite laminate with different interface fiber orientations using an AE technique [7]. In this case, a fiberglass DCB composite test specimen was used. It was observed that the load–displacement curve and cumulative AE events seemed to be well correlated. Once again, a sharp jump in cumulative AE events was associated with damage initiation. Barile undertook a similar study to investigate mode I delamination growth for a DCB test specimen made of CFRP material [8] noting similar results to [7]. Saidane et al. investigated the failure mechanism of the Mode I inter-laminar fracture toughness of flax, glass, and hybrid flax-glass fiber woven composites using an AE technique [9] using the increase in the rate of the cumulative AE events to predict the initiation of damage. They divided the AE events into four clusters and tried to find the contribution of each cluster to the damage propagation.

Tabrizi et al. investigated the behavior of glass/carbon fiber hybrid composites under pure bending and tensile loading conditions also

^{*} Corresponding author.

E-mail address: s.khoshmanesh@tudelft.nl (S. Khoshmanesh).

using an increase in the rate of cumulative AE events as a sign of initiation of damage in a test specimen, [10]. Ali et al. used the same method to analyze the damage mechanism in woven carbon fabric laminates under a tensile test [11]. Ameur et al. investigated the identification of damage mechanisms of unidirectional carbon/flax hybrid composites using an AE technique [12]. They performed static and fatigue tension tests on test specimens consisting of unidirectional carbon and flax fiber plies with different stacking sequences to create different levels of damage, classifying the amplitude of AE event from low to high which were associated with four types of damage including matrix cracking, fiber–matrix de-bonding, delamination/fiber pull-out, and fiber breakage. Based on this assumption, they calculated the cumulative number of AE events and cumulative energy of AE events for each class. Haggui et al. used the same methodology as [12] to describe the damage mechanism in flax fiber reinforced thermoplastic composites [13]. Khademi et al. used wavelet analysis of acoustic emission signals to characterize damage in carbon/epoxy composites under a quasi-static tensile test [14].

Saeedifar et al. used AE and machine learning to characterize damage in an adhesively-bonded Bi-material joint [15] employing two different structural adhesives, ductile (Methacrylate-based) and brittle (Epoxy-based), to bond CFRP skins to a steel core. The fabricated joints were subjected to quasi-static tension load tests while damage evolution was monitored using AE. In order to distinguish and classify different damage mechanisms, different tests were conducted. Each test on the coupons was representative of one type of damage mechanism present in an adhesively-bonded Bi-material. The AE signals captured during these tests were used to train an ensemble bagged tree classifier. The same group used acoustic emission to assess low-velocity impact damage in a Carbon Fiber Reinforced Polymer (CFRP) composite plate [16]. The test specimen was subjected to a repeated quasi-static indentation test where a loading–unloading–reloading test profile with five repetitions was adopted. A Felicity Ratio (FR) was used to measure damage severity during loading. Pasco et al. studied crack growth during the cyclic fatigue loading of a double cantilever beam (DCB) specimen, consisting of two aluminum arms [17]. It was found that crack growth can occur both during loading and unloading, but only while the strain energy release rate is above a crack growth threshold value. It was concluded that to fully understand the link between the acoustic emission signals and the actual crack growth process, further research was necessary.

Round et al. investigated the static load and fatigue behavior of glass/epoxy composite laminates. The specimens were subjected to static loading and cyclic fatigue tensile tests and the AE events were recorded [18]. AE events based on the amplitude range were classified into four clusters. Each amplitude range was associated with one type of failure. The damage was divided into matrix cracking, matrix fiber de-bonding, delamination, and breakage with amplitude ranges of 45–65 dB, 65–80 dB, 80–90 dB, and greater than 90 dB, respectively. The contribution of each class to the damage propagation was estimated during the static loading and cyclic fatigue tension tests. Saeedifar et al. studied damage evolution in a CFRP composite material under a quasi-static indentation loading using AE [19]. A sentry function (the logarithm of the ratio of mechanical energy given to the test specimen during loading to the AE energy due to the damage) was used to characterize damage propagation. Different AE event clustering methods were used to evaluate the contribution of different damage mechanisms during testing. It was concluded that a hierarchical model was a good candidate for clustering AE events related to three damage mechanisms, i.e., matrix cracking, fiber breakage, and delamination. The same approach was used to detect scarcely visible damage in CFRP composite material [20]. Saidane et al. Malpot et al. and Zhou et al. used clustering of AE events to monitor damage propagation in hybrid flax-glass fiber composites, woven glass fiber reinforced plastic (GFRP), and woven CFRP under quasi-static tension, fatigue tension, and quasi-static tension tests, respectively [9,21,22].

Tang et al. attempted to classify AE events from a wind turbine blade during a fatigue test [23]. K-means clustering was used to classify AE events measured during the fatigue test of a 45.7 m long wind turbine blade loaded in the flap-wise direction into four different classes. These classes were related to the different damage mechanisms that occurred during the fatigue test including matrix cracks, delamination, de-bonding, and fiber breakage.

The studies described above rely primarily on observing an abrupt change in the rate of generation of accumulated AE events during constant loading conditions to identify damage. This has limitations in a real loading scenario where a wind turbine blade is operating in turbulent and time-varying wind conditions. Furthermore, it is difficult to monitor progressive damage. To address these limitations, in this paper, we explore the possibility of monitoring the spatial distribution and local density of AE events to identify damage initiation and monitor damage accumulation during the fatigue life of a representative composite test specimen.

Sørensen et al. conducted an experimental study at Risø National Laboratory to investigate damage evolution in wind turbine blades [24]. They subjected a 25 m wind turbine blade (type V52, provided by Vestas Wind Systems A/S) to full-scale extreme loads and cyclic loading corresponding to a 20-year fatigue life. Seven types of damage were observed, with one major type being damage formation and growth in the adhesive layer joining the skin and main spar flanges (skin/adhesive debonding and/or main spar/adhesive layer debonding). Sundaresan et al. also conducted a static test on a 9 m wind turbine blade and demonstrated that the high-pressure skin, spar cap, and shear web are areas prone to damage in wind turbine blades [25]. Mishnaevsky et al. reviewed the root causes and mechanisms of damage and failure in wind turbine blades [26]. This review, along with two others by Shohag et al. [27] and Ciang et al. [28], indicated that one critical area prone to damage is the upper spar cap/flange of the wind turbine blade. Mishnaevsky et al. concluded that the strength and durability of wind turbine blades are largely controlled by the strength of adhesive joints. These studies highlight the critical role of the spar cap-shear web adhesively bonded connection in wind turbine blades. Zarouchas et al. Sayer et al. and Khoshmanesh et al. conducted experimental investigations into the evolution of fatigue damage in this joint [2,29,30].

Impact during transportation is one of the sources of damage to wind turbine blades. However, the effect of initial impact with varying energy levels on fatigue damage propagation in a thick adhesively bonded connection has not been previously explored. In this paper, we present an experimental study to investigate the effect of this initial impact on fatigue damage accumulation in the adhesive joint. Additionally, we examine the feasibility of using acoustic emission measurements to monitor damage accumulation by analyzing their spatial distribution and local characteristics.

2. Methodology

To investigate the effect of impact damage on the fatigue damage accumulation process in a spar cap-shear web adhesively bonded connection of a wind turbine blade, three cases of impact damage were instigated using a gas cannon on test specimens representative of this bonded connection. These three cases were chosen to induce different levels of initial damage on the test specimens.

The test specimens were then subjected to fatigue tension tests with a stress ratio, R (ratio of minimum load amplitude to maximum load amplitude) equal to 0.1 and a fatigue cycling frequency of 3 Hz. Two acoustic sensors were attached to the top and the bottom of the test specimens to measure AE events. An AE event (elastic wave) is generated in a material when the bonds between atoms are broken. This happens when the test specimens are subjected to a load. To identify the spatial distribution and local density of generated AE events the test specimens were divided into a number of spatial elements subsequently referred to as bins. The cumulative number of AE events generated in

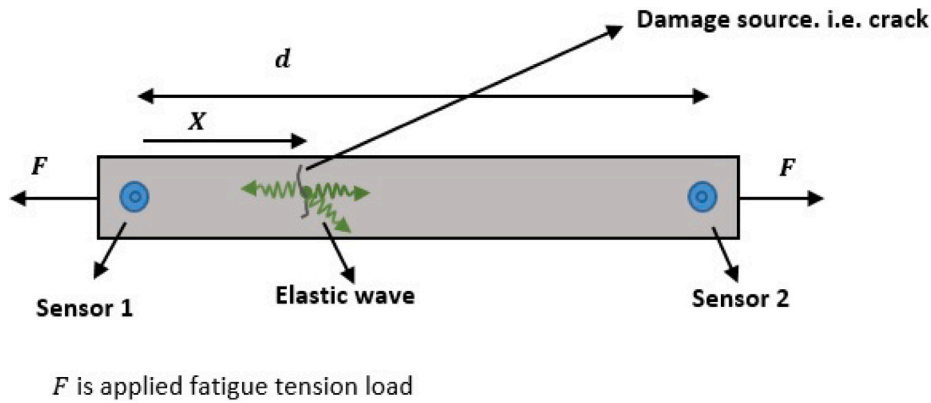


Fig. 1. Schematic illustration of the test specimen in a tension fatigue load with a damage source, i.e. crack and two sensors to identify the damage source.

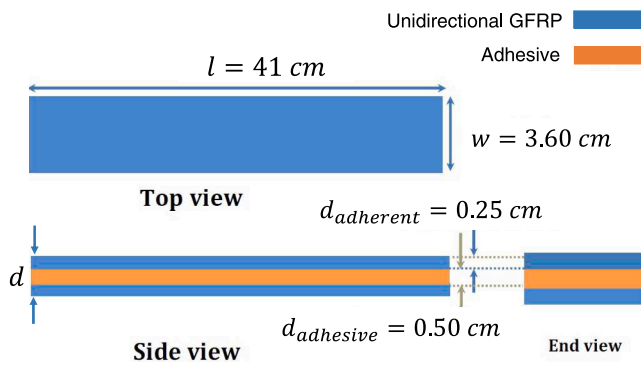


Fig. 2. Schematic illustration of a test specimen.

each bin during the fatigue tests was determined. The difference in the arrival time of AE events recorded by two sensors was used to locate the source of damage [31]:

$$X = (d - V \cdot \Delta t) / 2 \quad (1)$$

Referring to the schematic of a test specimen subjected to a fatigue tension load F as shown in Fig. 1, X is the distance of the source of an AE event from Sensor 1, V is the velocity of the elastic wave associated with the event, Δt is the difference in the time of arrival of the event at Sensor 1 and Sensor 2 and d is the distance between the two sensors.

The cumulative normalized number of AE events, $N_n(t, i)$, detected in bin i at time t is given by:

$$N_n(t, i) = \frac{N(t, i)}{N_o} \quad (2)$$

where $N(t, i)$ is the absolute number of the AE events generated since the beginning of the fatigue test in the i th bin of each test specimen and N_o is the total number of the AE events generated throughout the entire length of a test specimen during its fatigue life. This measure gives an indication of the spatial location of the damage to the test specimen.

A high-resolution camera was used to photograph the damaged test specimens. Using the pictures of the damaged test specimens at different fatigue life cycles the effect of impact on the fatigue damage accumulation process was investigated.

An acoustic emission technique was used to detect the initial impact damage on the test specimens. This was done by dividing the test specimens into a number of spatial elements subsequently referred to as bins. The cumulative number of AE events generated in each bin during the initial phase of damage was determined. The bin with the largest number of AE events was expected to be the area where impact damage was initially instigated. To monitor the fatigue damage accumulation

process during the fatigue life, the cumulative spatial distribution of AE events within the test specimens was analyzed.

3. Experimental set up

3.1. Test specimen

The test specimen used in the research was an adhesive joint representative of a spar cap-shear web adhesively bonded connection that would be seen in a wind turbine blade. Several test specimens were manufactured. Each test specimen consisted of two skins of unidirectional fiberglass which were made by the infusion of epoxy resin into three layers of unidirectional (UD(0)) fibers. These two skins were then bonded together by a layer of adhesive. The material properties of all components for manufacturing the test specimens are given in Table 1 and a schematic illustration of a test specimen is shown in Fig. 2.

3.2. Impact cases

Different levels of impact damage were imposed on the test specimens using a gas cannon. A gas cannon uses compressed air to shoot a projectile with a specified energy using a regulator to adjust the air pressure. There is also an air relief valve that can be opened manually to fine-tune this pressure. Once the pressure is set to the desired level, to which the velocity of the projectile is proportional, a valve is opened and the projectile is propelled via a cylinder to the intended target. The experimental set-up using the gas cannon is shown in Fig. 3.

In Fig. 4, images of the projectile before, during and after hitting the test specimen are shown.

Three impact cases (Case 1, Case 2, and Case 3) representing different levels of impact damage were imposed on the test specimens. Photos of the impact-damaged specimens are shown in Fig. 5. The velocity of each projectile was measured using a high-speed camera. The characteristics of each impact including projectile properties, velocity, and energy level are given in Table 2.

For each impact case, three test specimens were damaged giving a total of nine test specimens used for the experiment. The test specimens after impact are shown in Fig. 5. In this figure, the nine test specimens are divided into three sets with each set showing the three different cases of impact damage.

3.3. Acoustic measurement

The impact damaged test specimens were subjected to a tension fatigue test using a 100 kN hydraulic fatigue rig under load control as illustrated in Fig. 6. The reason for conducting a fatigue tension test is that this test represents the loading condition that would be experienced by a joint that is used in the upper part of a spar cap

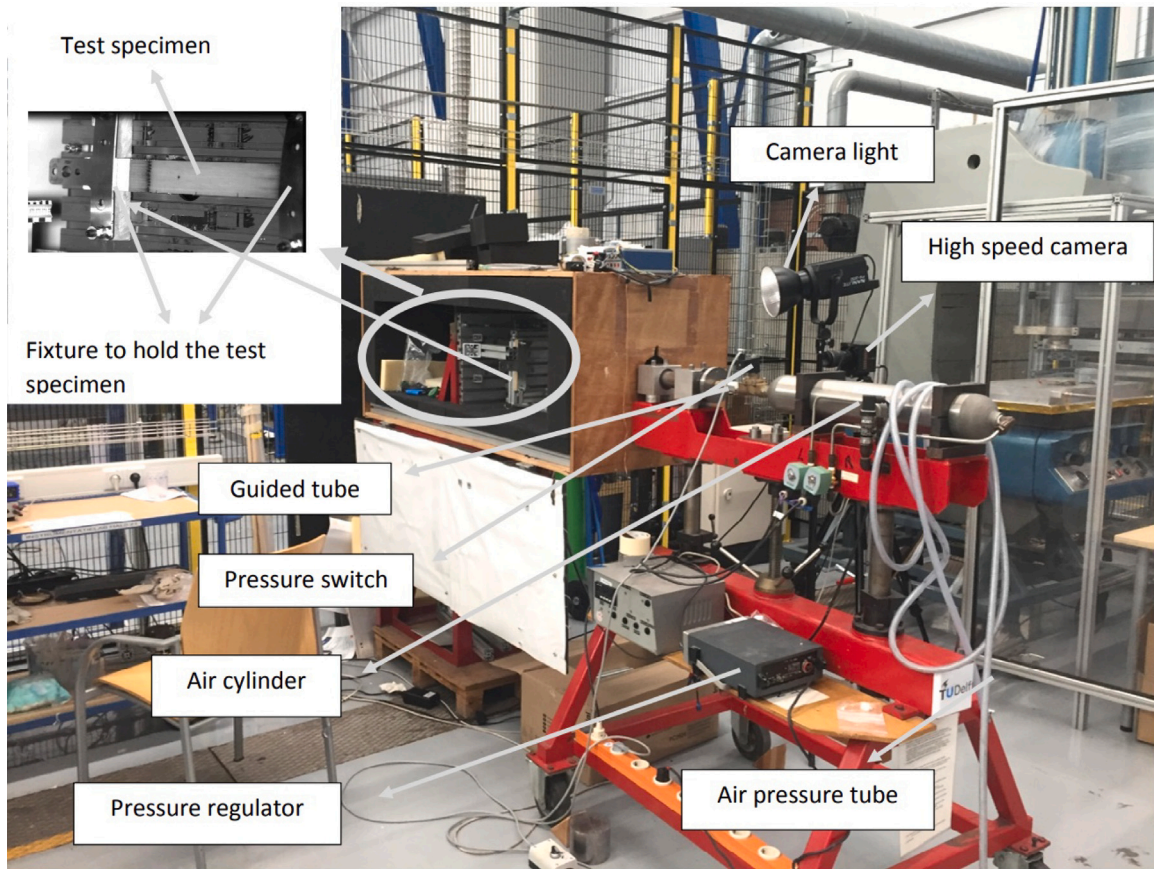


Fig. 3. Experimental set-up using the gas cannon to impose impact damage on the test specimens.

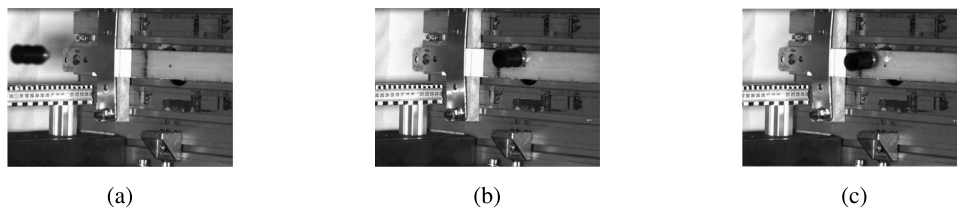


Fig. 4. Images of the projectile (a) before (b) during and (c) after hitting the test specimen.

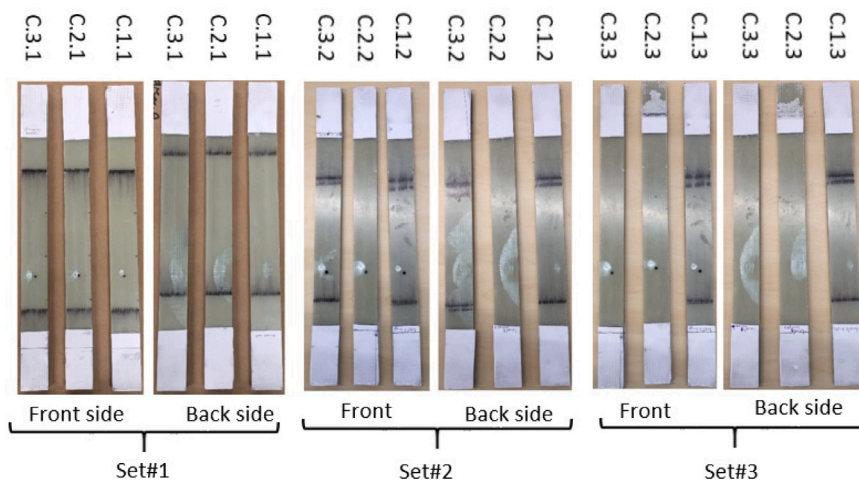


Fig. 5. The set of test specimens following the initial impact damage showing both front and back.

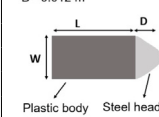
Table 1

Mechanical properties of the different materials used for the manufacturing of the test specimens where: E_Y = Young's Modulus, σ_u = ultimate strength and ρ = volume density.

Material specification			E_Y (GPa)	σ_u (MPa)	ρ (g/cm ³)
Adhesive	Resin	Epoxy Epikote Resin MGS BPR135G2	5.5	75	1.1-1.2
	Curing agent	Epoxy Epikure Curing Agent MGS BPH1355G			
Adherent	Resin	Epoxy Epikote Resin MGS RIMR135	22.8	376	1.3-1.17
	Curing agent	Epoxy Epikure Curing Agent MGS RIMH 137			0.99
	UD fiber glass	Fiber glass cloth UD (0), 1210 g/m ² , S14EU960			–

Table 2

Impact test characteristics and projectile properties.

Energy level	Test specimen No	projectile velocity (m/s)	Energy (Joule)	Projectile properties
Case 1	C.1.1	21.1	15.7	Weight= 0.0675 kg L=0.02 m W=0.01 m D= 0.012 m 
	C.1.2	22.7	17.39	
	C.1.3	21.7	15.89	
Case 2	C.2.1	25.86	22.57	
	C.2.2	27.27	25.10	
	C.2.3	26.31	23.36	
Case 3	C.3.1	31.9	34.34	
	C.3.2	30.3	30.44	
	C.3.3	30.6	31.6	

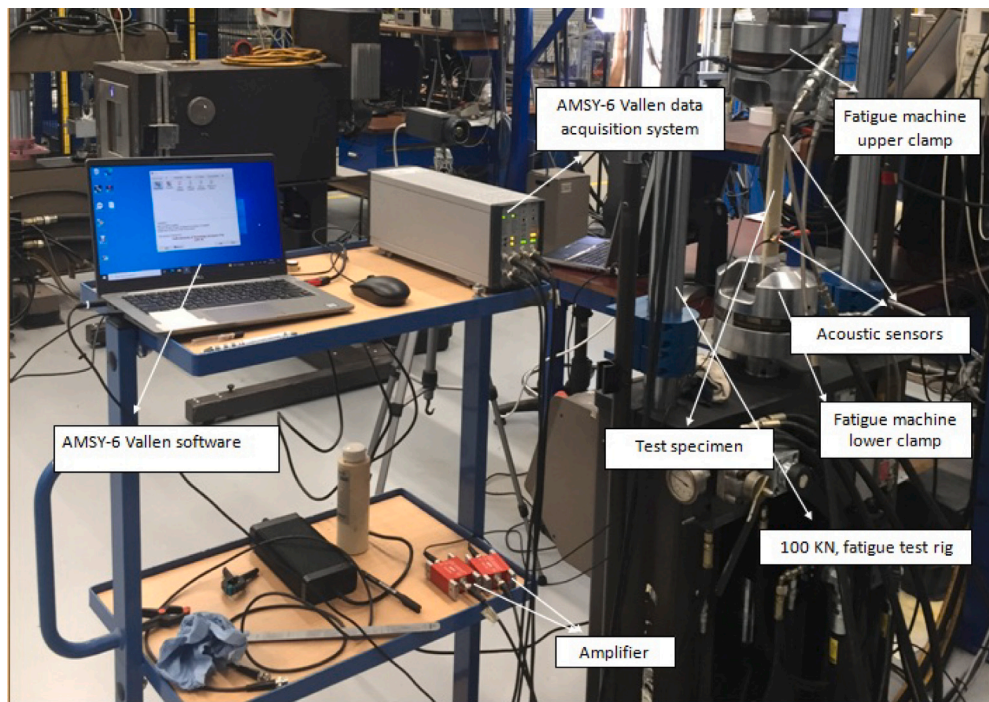


Fig. 6. The AE measurement and fatigue test set-up.

shear web assembly of a wind turbine blade. This has been justified and discussed in section 4.1 of a previous study [2]. To capture AE events, during the fatigue tests, two broadband, resonant-type, and single-crystal piezoelectric transducers from Vallen Systeme GmbH, AE1045SVS900M, with two external 34 dB pre-amplifiers were used. The optimum operating frequency range of the AE sensors was [100 – 900] kHz. To record the AE events, an AMSY-6 Vallen, 4-channel AE system with a maximum sampling rate of 10 MHz was used. The threshold of the receiving AE signals, sampling rate, Duration Discrimination Time (DDT) and Rearm Time (RAT), were 60 dB, 2 MHz, 200 μ s and 400 μ s, respectively. Sonotech Ultrasonic couplant was applied between the sensor and specimen surfaces to get an appropriate acoustic coupling. The functionality of the AE sensors and the data acquisition system was checked by performing a pencil lead break test according to the ASTM E976 standard. The test setup is shown in Fig. 6.

4. Results and discussion

4.1. Fatigue damage accumulation process based on high-resolution photos

During each fatigue tension test, photos of the test specimens by a high-resolution camera at different fatigue load cycles are taken. As the three test specimens showed a similar pattern of damage, the results of only one test specimen for each case of impact damage is shown.

The fatigue damage accumulation process for C.1.1 is shown in Fig. 7. As can be seen from this figure, damage initiates with cracks in the adhesive during the early stage of the fatigue test. This is the initiation phase of damage (Phase I). Cracks in the test specimen are transverse and initiate within the adhesive. They grow transversely and reach the interface of laminate and adhesive causing de-bonding of the laminate from the adhesive. Each horizontal white line seen

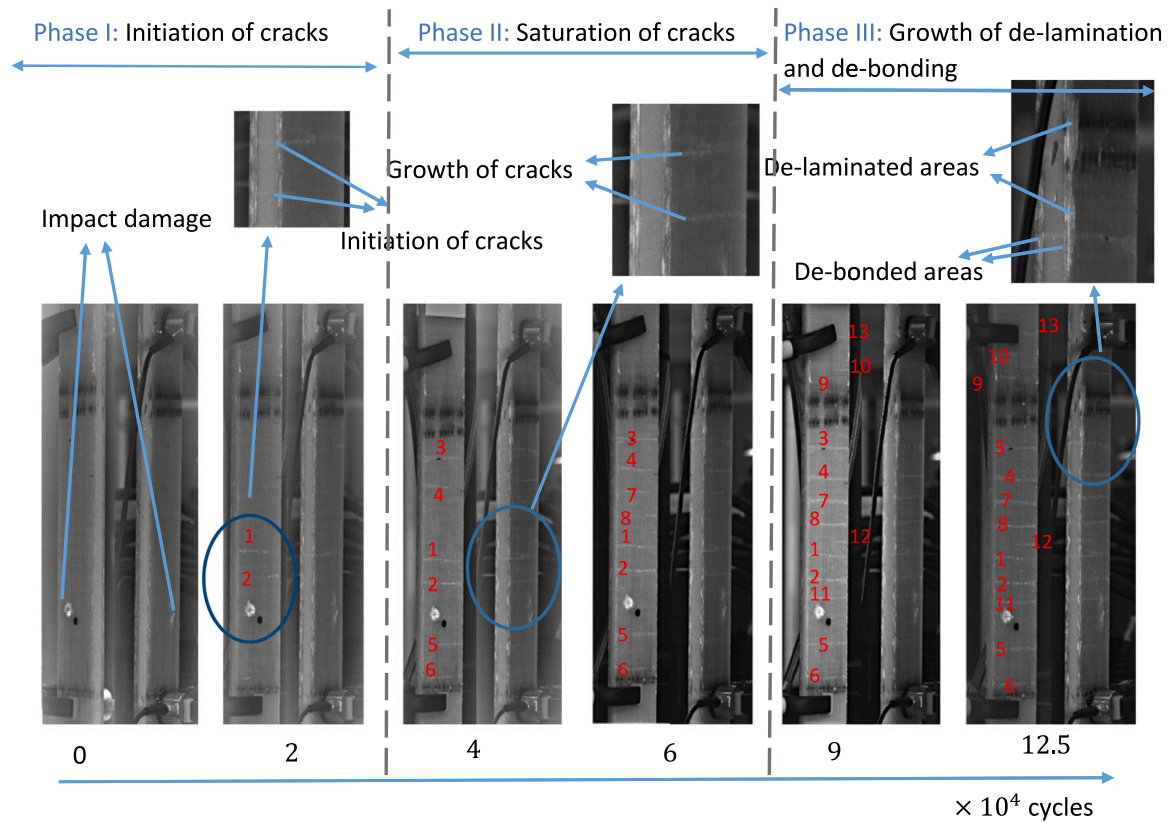


Fig. 7. Damage propagation in one of the test specimens (C.1,1) subjected to the low energy level impact. The left image of each pair shows the front where impact occurred and the right image is the back. Each photo shows an AE sensor attached at the top and bottom of each test specimen. Cracks which develop during the fatigue test are labeled with numbers for clarity.

in Fig. 7 (at the position where a crack has occurred) is a de-bonded area. The width of each line shows how far the crack has progressed in depth within the test specimen. As the number of fatigue load cycles increases, cracks become widespread throughout the test specimen and this trend continues until the number of cracks reaches a saturation level. This phase of damage is known as the crack saturation level (Phase II). During Phase III, cracks deepen and consequently the de-bonded areas increase. The de-bonded areas grow as the number of fatigue load cycles increases. Finally, the de-bonded areas become connected leading to failure of the test specimen. The first crack is not within the impact zone and subsequent cracks which appear are not associated with this zone. This indicates that the fatigue damage accumulation process was not influenced by the size and location of the impact damage and it is identical to that seen in previous tests on an undamaged test specimen [2].

The fatigue damage accumulation process for C.2.1 is shown in Fig. 8. In this case, crack initiates close to the impact zone. As damage propagates, a higher crack density than in other areas of the test specimen is observed near the impact zone. The de-laminated area in the impact zone also grows more than elsewhere in the test specimen during the fatigue test ultimately resulting in failure in this zone.

The fatigue damage accumulation process for C.3.1 is shown in Fig. 9. Similar to C.2.1, the early cracks occur at the impact zone and the crack density in this zone is higher than other parts of the test specimen. In this case, the de-laminated area around the impact zone grows more extensively and faster compared with C.2.1 leading ultimately to failure in this zone.

4.2. Early detection of impact damage

To detect the impact damage during Phase I of the fatigue test, the test specimens were divided into 2 cm bin lengths as shown in

Fig. 10. Each impact position was 4.2 cm from the lower AE sensor as shown in the photos in Figs. 7 to 9. The length (L) of the de-laminated area surrounding the impact point in the lateral direction depends on the impact energy level, varying from 2 cm to 8 cm. To detect the impact damage in the early stage, the normalized number of AE events during Phase I of damage in the fatigue test for each bin was calculated. Because impact damage accelerates the generation of AE events, it was expected that the bins located in the impact zone would have the highest number of events. In this section, results for all three test specimens subjected to the same level of impact energy are presented to show the degree of variability in damage localization.

4.2.1. Case 1 impact

The total number of normalized AE events by bin during Phase I of the fatigue test for the test specimens subjected to the Case 1 impact is shown in Fig. 11.

It can be seen for C.1.1 that the 0–2 cm bin (inside the impact zone) was not the most damaged section but rather the 20–22 cm bin, far from the impact area. For C.1.3, the most damaged section was located between 20–22 cm which is also far from the impact zone.

4.2.2. Case 2 impact

The corresponding results for the test specimens subject to the Case 2 impact are shown in Fig. 12. It can be seen that the bins between 0–2 cm and 4–6 cm are the most damaged sections of C.2.1 which are relatively close to or within the impact area respectively.

The results for C.2.2 and C.2.3 show peaks in normalized events in bins 2–4 cm and 4–6 cm, respectively, which are inside the impact zone.

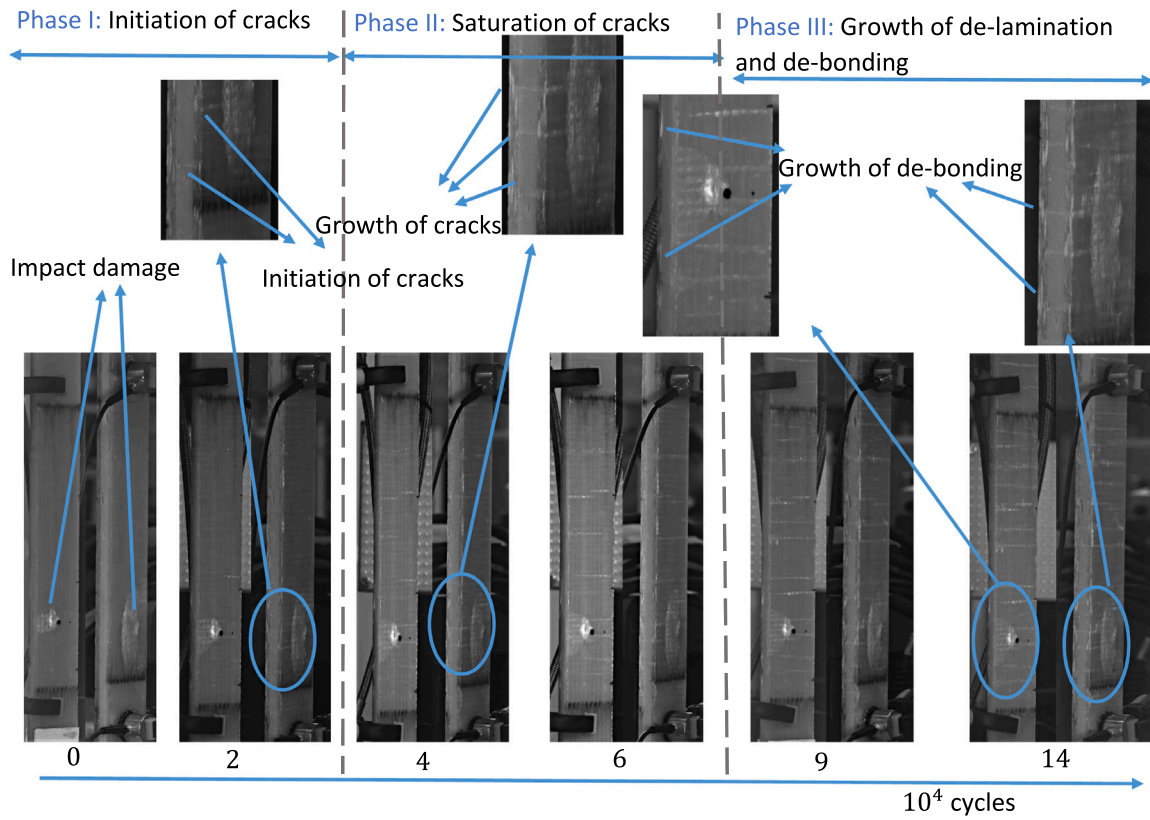


Fig. 8. As Fig. 7 but for C.2.1.

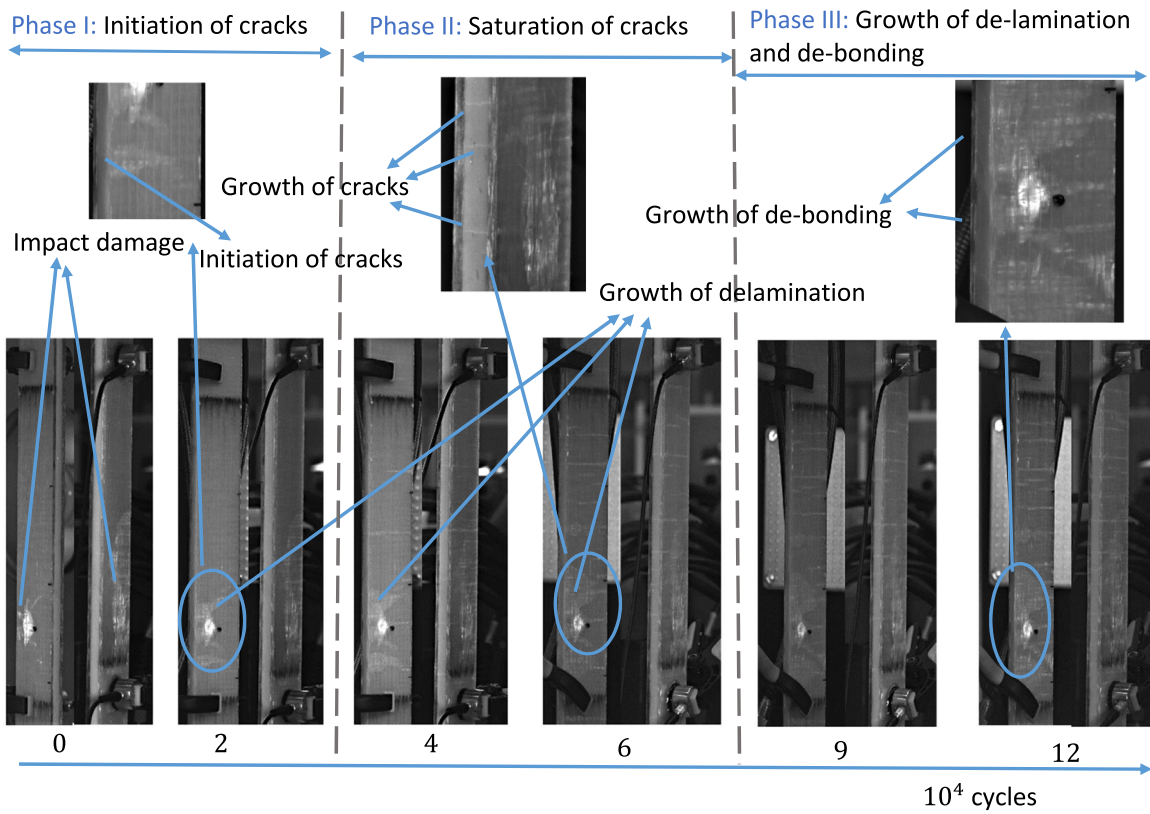


Fig. 9. As Fig. 7 but for the C.3.1.

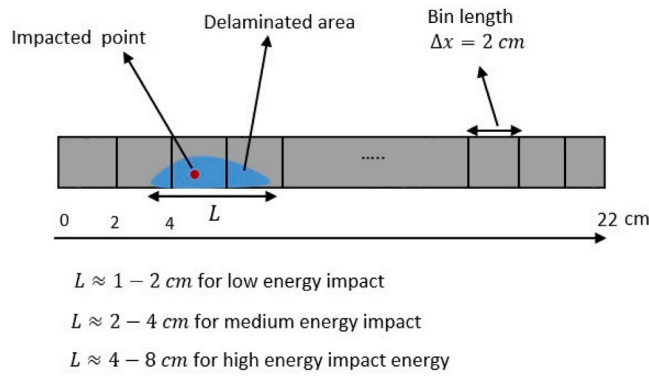


Fig. 10. Schematic illustration of the test specimen divided into 2 cm bins. Also illustrated are the impact point, and length of de-laminated area (L) in the lateral direction.

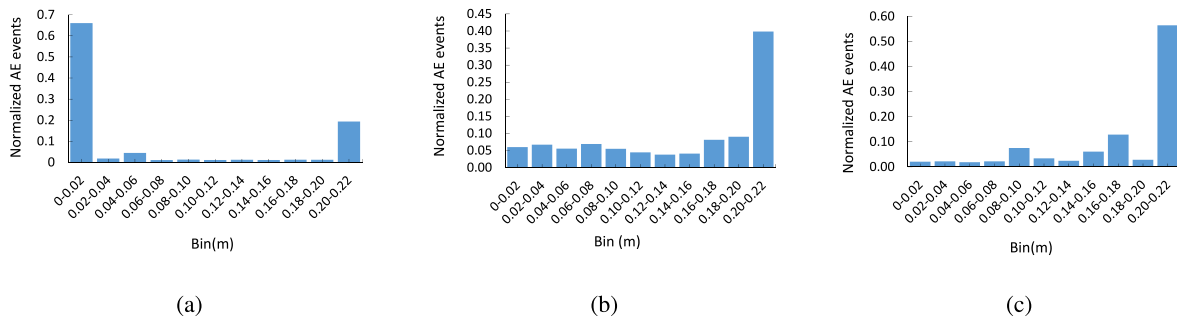


Fig. 11. The total number of normalized AE events by bin at the end of Phase I of the fatigue test for the three test specimens subjected to the Case 1 impact: (a) C.1.1 (b) C.1.2 (c) C.1.3.

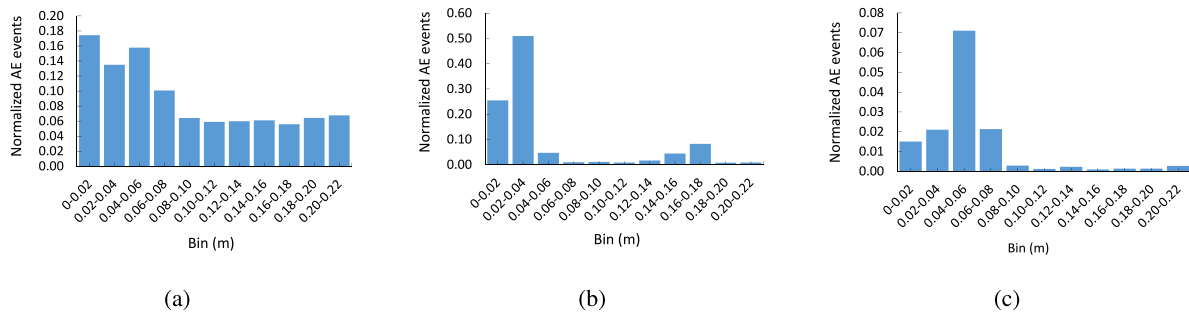


Fig. 12. The total number of normalized AE events by bin at the end of Phase I of the fatigue test for the three test specimens subjected to the Case 2 impact: (a) C.2.1 (b) C.2.2 (c) C.2.3.

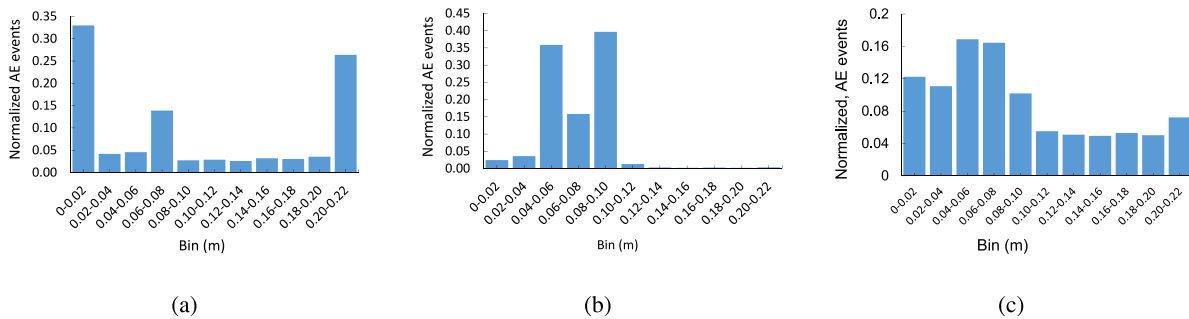


Fig. 13. The total number of normalized AE events by bin at the end of Phase I of the fatigue test for the three test specimens subjected to the Case 3 impact: (a) C.3.1 (b) C.3.2 (c) C.3.3.

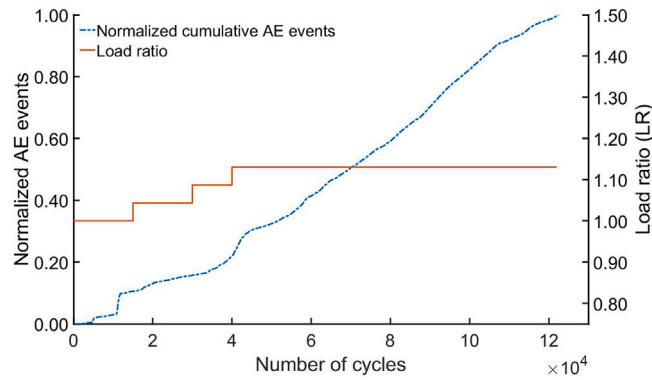


Fig. 14. Normalized AE events during the fatigue test for C.1.1.

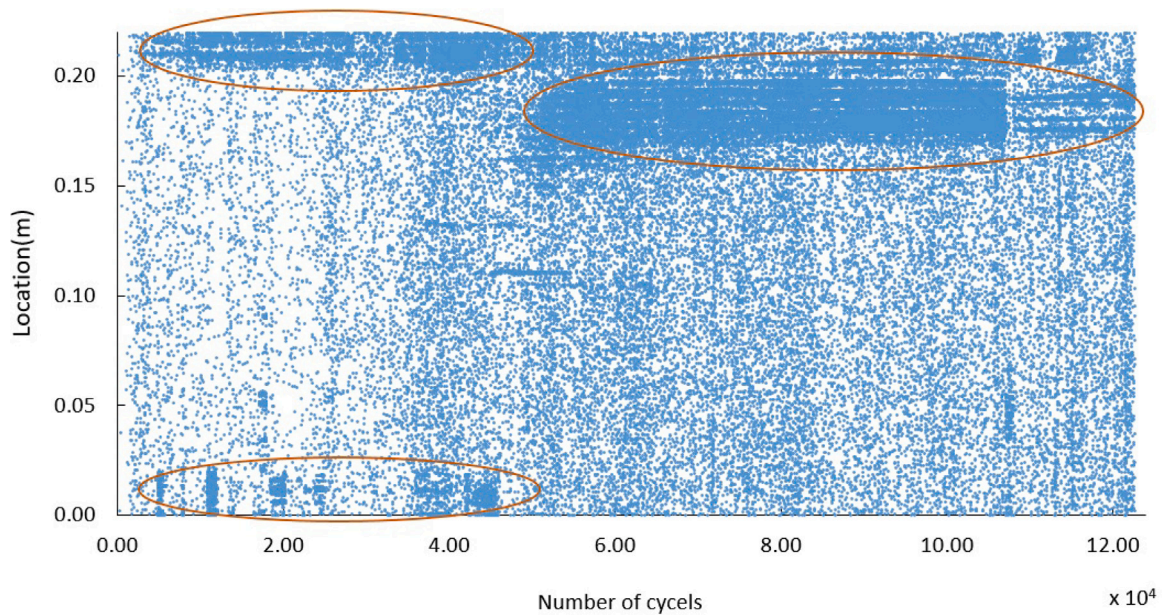


Fig. 15. Spatial distribution of AE events during the fatigue life, for C.1.1.

4.2.3. Case 3 impact

Fig. 13 shows the corresponding results for the test specimens subjected to the Case 3 impact. C.3.1 shows the largest peak in normalized events in the bin close to the bottom of the specimen (0–2 cm), with another smaller peak at the top (20–22 cm). C.3.2 and C.3.3 show the largest number of normalized events in the bins spanning the sections from 4–10 cm which encompass the impact zone.

4.2.4. Correlation between impact and fatigue damage

From the results of the three cases of damage, the AE measurements would seem to broadly confirm the levels of visual damage observed in Figs. 7–9. For the test specimens subjected to the Case 1 impact, fatigue damage is not correlated with the area of the initial impact. For the test specimens subjected to the Case 2 and Case 3 impacts, fatigue damage does appear to initiate close the area of impact, though there is some variability between the test specimens. In some cases, peaks in fatigue damage occur at the ends of the specimens which may be due to the gripping force induced by the end clamps where damage initiation and growth is facilitated.

4.3. Monitoring of the fatigue damage accumulation process by using the spatial distribution of AE events

During the fatigue tension tests, the amplitude of the load increases gradually to induce damage and facilitate its growth. The change in the

generation of AE events can be a sign of damage in the test specimen during the fatigue tension test. But the increase in load also increases the generation of AE events, the phenomenon known as the Kaiser effect,[32]. The Kaiser effect increases the AE generation homogeneously within the test specimens. Therefore, to localize damage, the local density of AE events in a specimen should be considered alongside an indicator of the load. For this purpose a load ratio (LR) can be defined:

$$LR = \frac{F}{F_i} \quad (3)$$

Where F is the load during the fatigue test and F_i is the initial load at the start of the fatigue test. The load ratio is increased during the fatigue test to assess the effectiveness of using the spatial distribution of AE events for identification and monitoring of the fatigue damage accumulation under variable conditions. In addition, increasing the load ratio causes the development of fatigue damage propagation at a faster rate. This reduces the required time for the experimental test and the storage space needed for the acoustic data.

4.3.1. Case 1 impact

Fig. 14 shows temporal changes in normalized AE events and load ratio during the fatigue test for C.1.1. This gives an indication of where changes in the load give rise to an increase in AE event generation, but

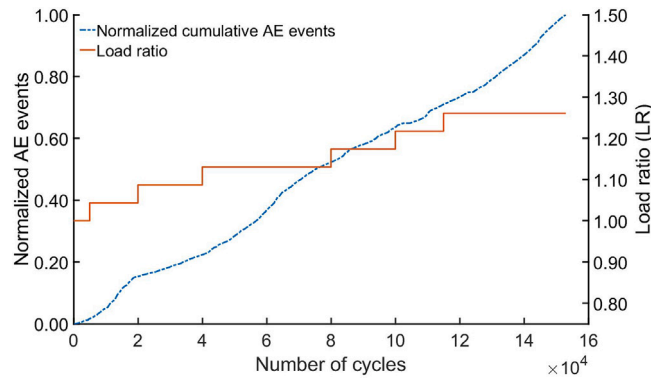


Fig. 16. As Fig. 14 but for the C.1.2.

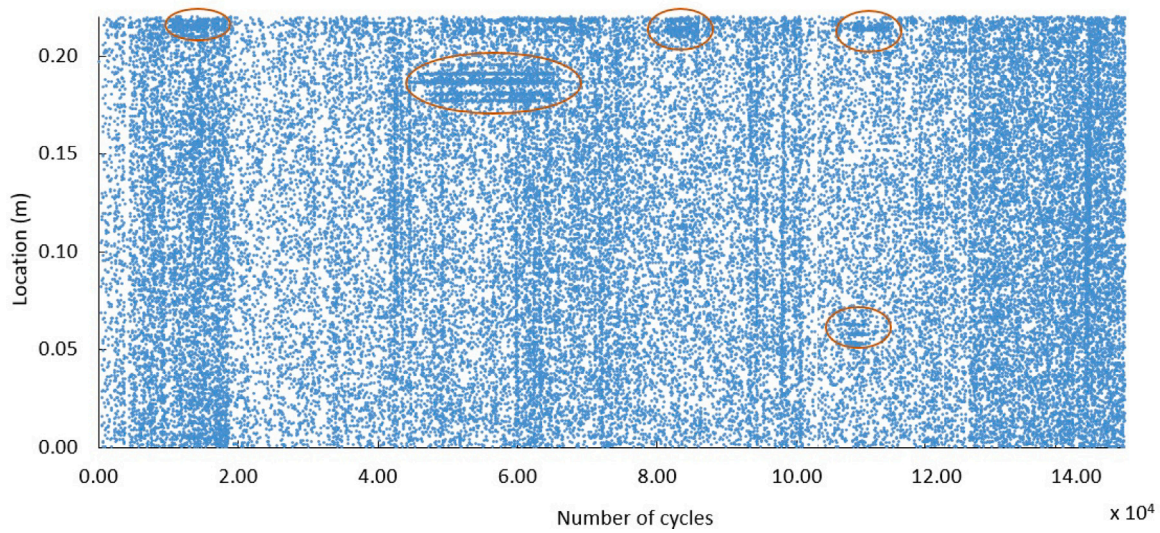


Fig. 17. As Fig. 15 but for C.1.2.

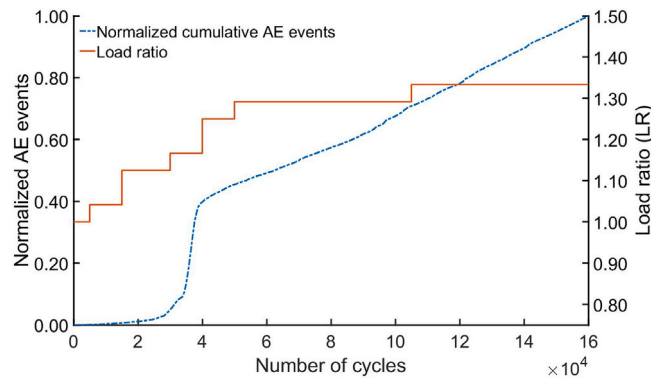


Fig. 18. As Fig. 14 but for C.1.3.

also shows where damage is accelerating where it is not necessarily associated with a change in the load. Fig. 15 shows the corresponding spatial density of normalized AE events. The damaged sections can clearly be seen during the fatigue life cycle marked in red. Initially, the [0–2] cm and [20–22] cm sections of the test specimen show significant damage. As the fatigue test progresses and damage propagates in the test specimen, the [17–20] cm section of the test specimen show significant damage. It is therefore clear that throughout the full fatigue test, the location of the fatigue damage is not associated with the impact zone.

Fig. 16 shows the changes in normalized AE events and load ratio during the fatigue test for C.1.2. The corresponding spatial density of AE events for this test specimen can be seen in Fig. 17. Similar results are seen compared to C1.1 and if anything, the damage is quite uniformly distributed throughout the test specimen for the duration of the fatigue test. Fig. 18 show the changes in normalized AE events and load ratio during the fatigue test for C.1.3 and Fig. 19 shows the corresponding spatial density of AE events. There a notable increase in events at around 3.5×10^4 cycles which corresponds to areas of damage indicated in red in Fig. 19, but otherwise damage in this case is quite

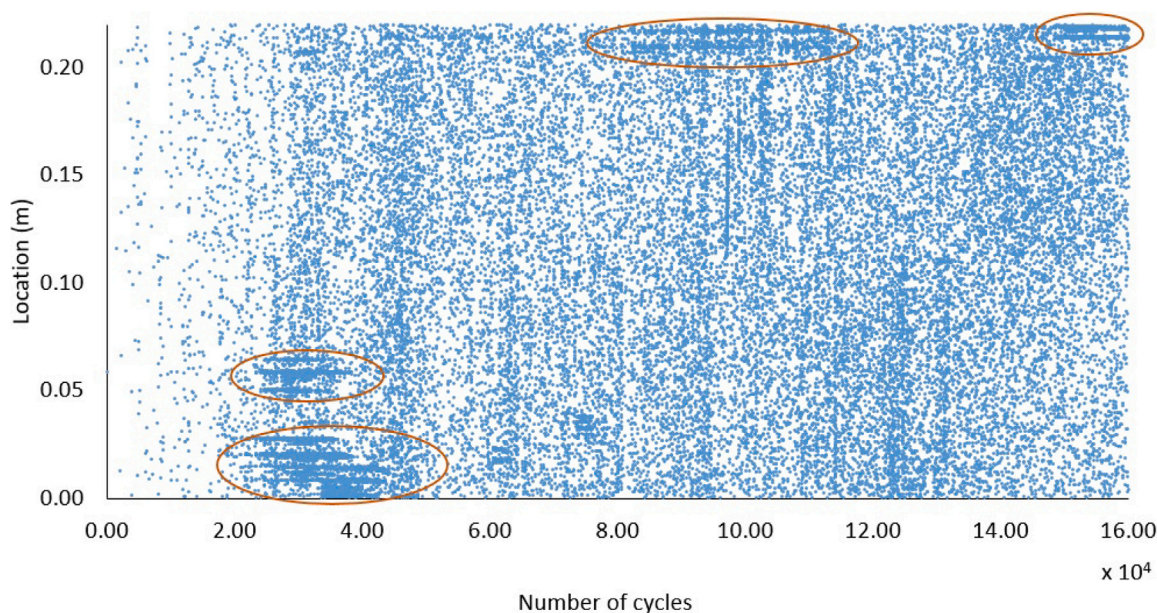


Fig. 19. As Fig. 15 but for C.1.3.

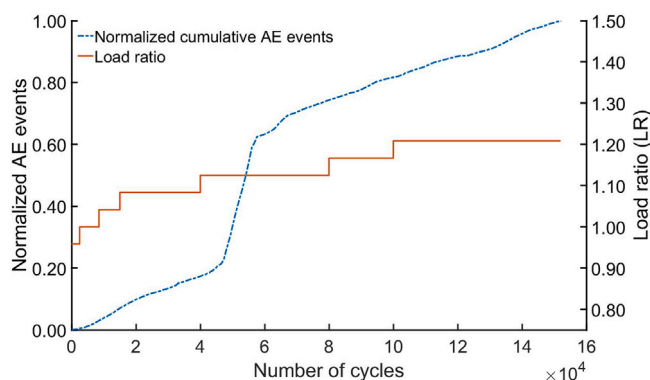


Fig. 20. Normalized AE events during the fatigue test for C.2.1.

uniformly distributed and not associated with the location of the impact damage.

4.3.2. Case 2 impact

Figs. 20 to 25 show the corresponding results for the test specimens subjected to the Case 2 energy impact. The increase in the density of AE events shows the damaged area. Continual growth in damage (higher density of AE events) within the impact zone for C.2.2 and C.2.3 can be seen until the end of the fatigue tension test. For C.2.1, the damage is initiated in the impact zone and then as the number of fatigue load cycles increases, it propagates to other sections of the test specimen. This propagation can be seen in Fig. 21 between load cycles 4×10^4 and 6×10^4 .

4.3.3. Case 3 impact

Figs. 26 to 30 show the corresponding results for the test specimens subjected to the Case 3 energy impact. Similar results as for the Case 2 energy impact can be seen here. Only for impact energy case 3. Only for C.3.3, there is no significant change in the spatial density of AE events in the impact zone, at the beginning of fatigue test as seen in Fig. 31. However, as the number of fatigue load cycles is increased, growth of the damage in the initial impact zone can be seen. This behavior is in slight contrast to the results seen for C.3.1 and C.3.2.

4.3.4. Summary of the analysis of the AE event distribution

When analyzing the spatial density of AE events for the three different test cases, damaged sections of the test specimens could clearly be seen. The highest density of AE events showed the most damaged sections of each test specimen. For the Case 1 impact, damage accumulation is seen to be more or less spatially uniform, however, for Cases 2 and 3, damage accumulation is associated with the initial impact damage zone. For all cases, there is a significant increase in the density of AE events within the impact zone at the beginning of the fatigue tension test, indicating that significant damage has occurred in this area. Although, the spatial distribution of AE events does not completely match the visible damage seen in Section 4.1, it does identify those areas most affected by damage during the fatigue tension tests. Therefore as a limitation, this method cannot scan all damaged areas during the fatigue test. A potential source of error in this experiment can be a decrease in the functionality of acoustic sensors during the fatigue test. It can be prevented by testing the functionality of the AE sensor with a pencil break test before the start of each fatigue test. Although the functionality of AE sensors was verified before the start of each fatigue test for case 3 energy impact and for the fatigue test C.3.3 the spatial distribution of AE events was not as expected. It was expected to have a higher density of AE events in the impacted area during phase 1 of damage.

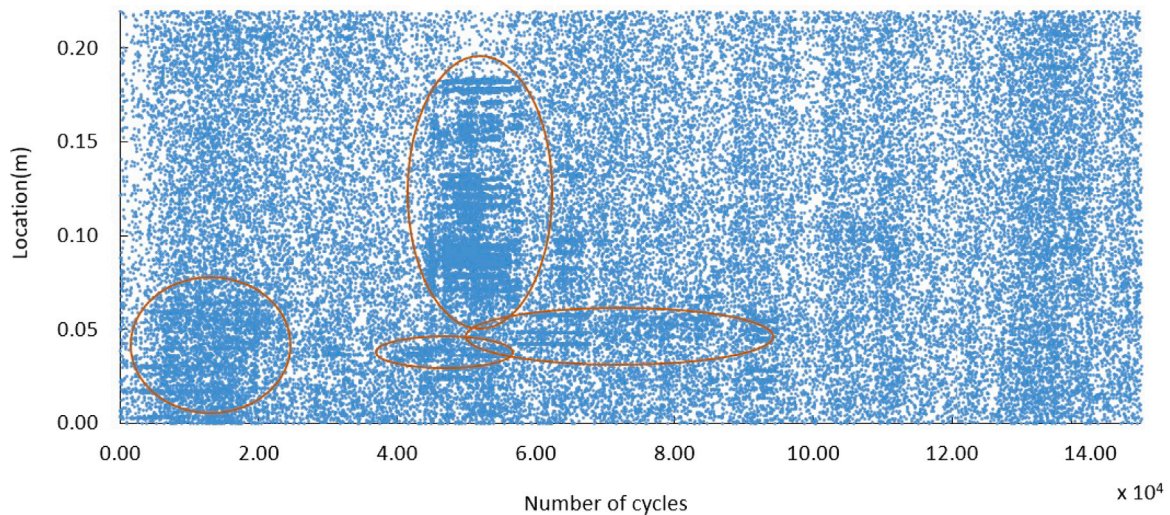


Fig. 21. Spatial distribution of AE events during fatigue life, for C.2.1.

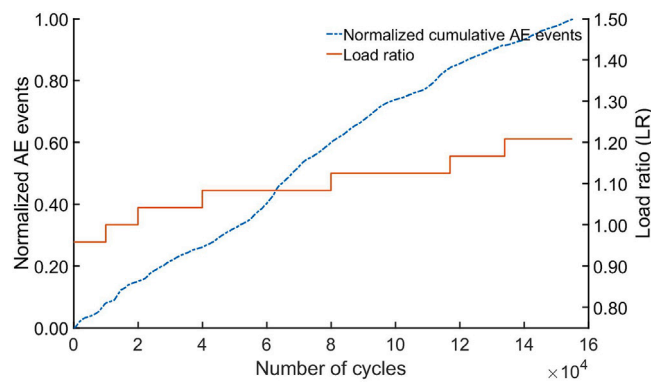


Fig. 22. As Fig. 20 but for C.2.2.

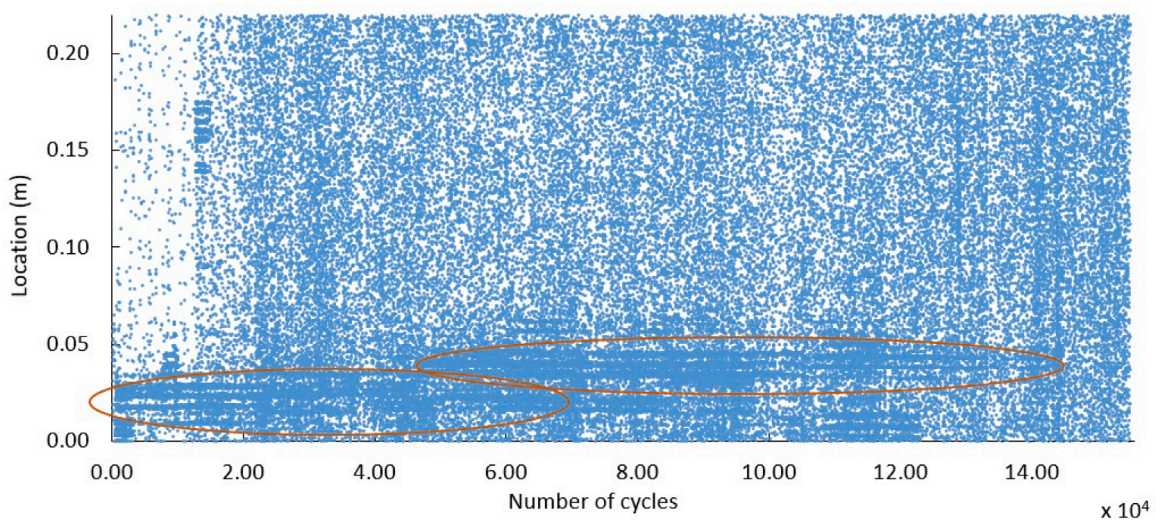


Fig. 23. As Fig. 21 but for C.2.2.

5. Conclusion

In this study, the effect of three levels of energy impact on the fatigue damage accumulation process for a thick adhesive joint representative of a spar cap to the shear-web adhesive joint of a wind turbine blade has been investigated. An acoustic emission technique has been

used to detect early damage and monitor the further accumulation of fatigue damage during a number of fatigue tests.

For the test specimens exposed to Case 1 impact with an average energy of 16.32 J, the fatigue damage accumulation process was not really influenced by the size and location of the impact damage. For test specimens exposed to Case 2 and Case 3 impacts with average energies

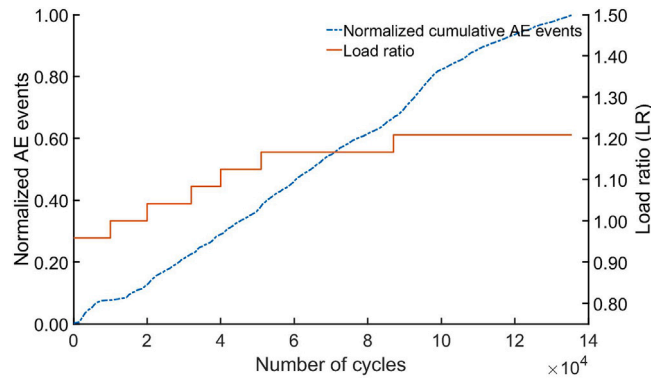


Fig. 24. As Fig. 20 but for C.2.3.

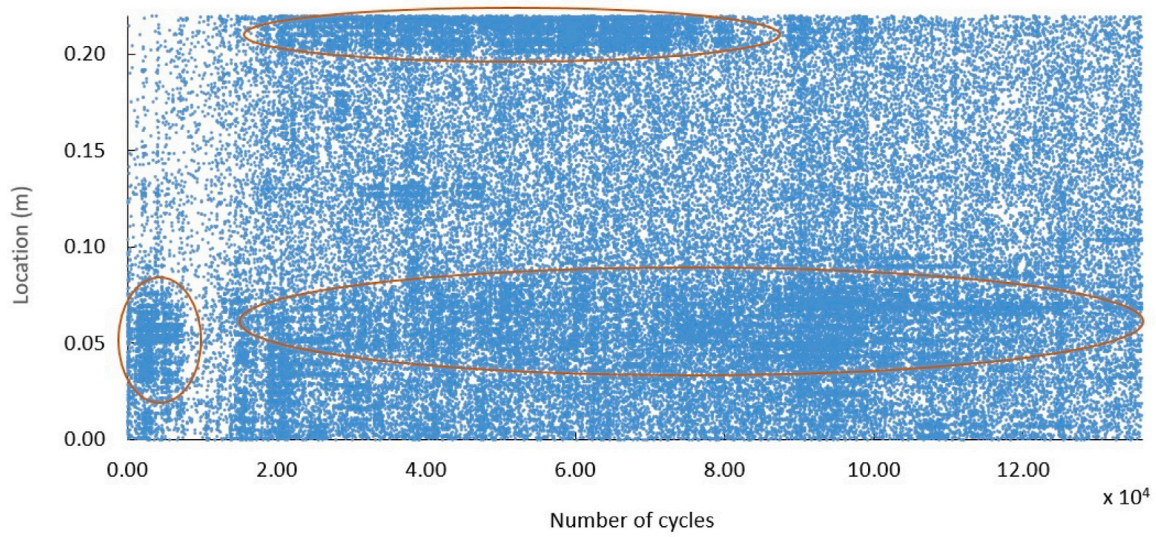


Fig. 25. As Fig. 21 but for C.2.3.

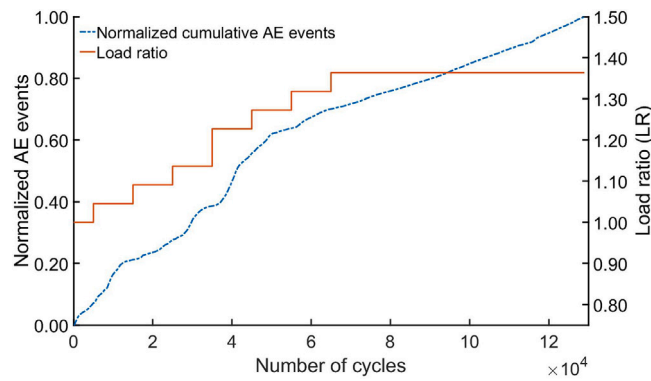


Fig. 26. Normalized AE events during the fatigue test for C.3.1.

of 3.68 J and 32.13 J respectively, the fatigue damage accumulation process was clearly influenced by the size and location of the impact damage. For these test specimens, higher crack density, greater delamination and de-bonding of adhesive from the laminate can be seen at the impact zone during the fatigue damage accumulation process. In addition, for the test specimens subjected to the Case 3 impact, the

delamination of the impact zone grows more extensively and faster through the test specimens than for the other impact cases.

The acoustic emission technique could detect damage in the impact zone during the early phases of the fatigue test for the test specimens subjected to Case 2 and Case 3 impacts. For the test specimen subjected to Case 1 impact, the acoustic emission technique did not detect

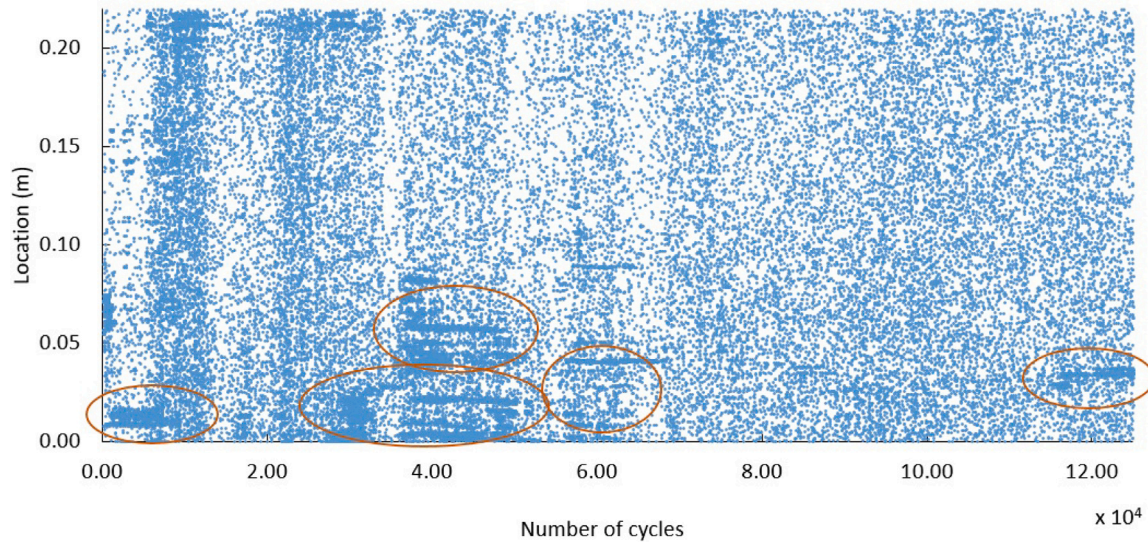


Fig. 27. Spatial distribution of AE events during the fatigue test for C.3.1.

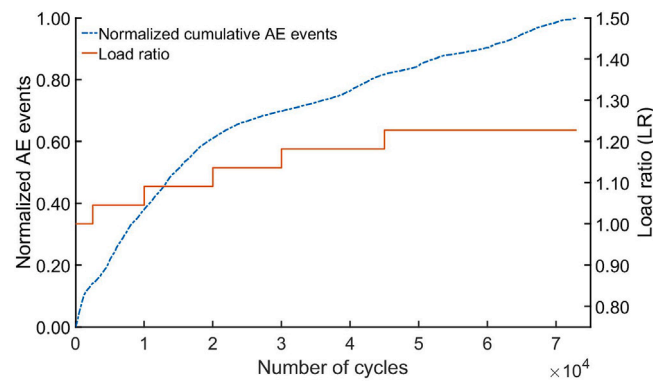


Fig. 28. As Fig. 26 but for the C.3.2.

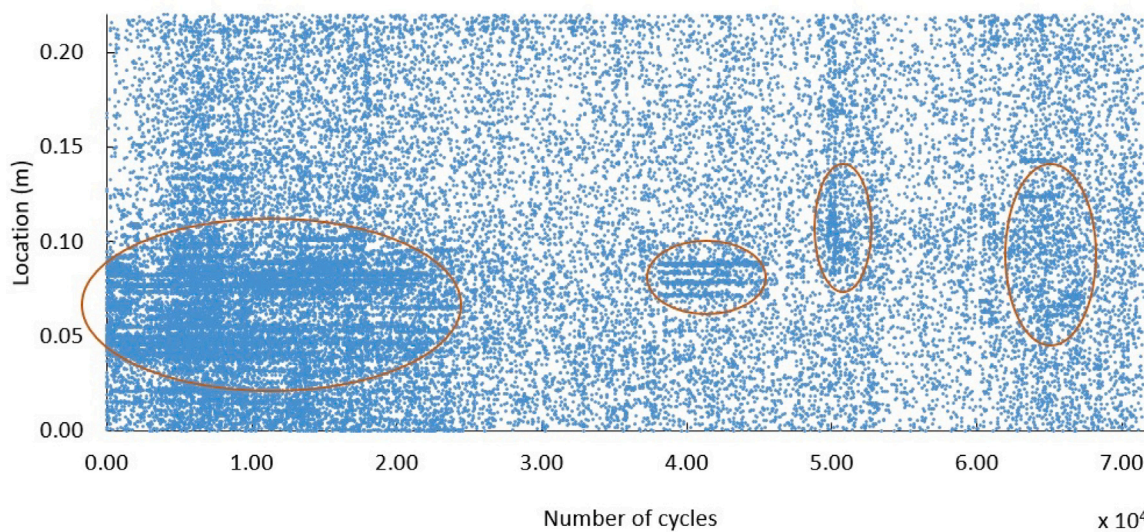


Fig. 29. As Fig. 27 but for the C.3.2.

damage in the impact zone in the early phase of the fatigue test. By contrast, other sections of the test specimens were seen to experience more damage during the tests.

The acoustic emission technique could show the accumulation of fatigue damage during the fatigue test in certain sections of the test specimens. For the test specimens subjected to Case 2 and Case 3

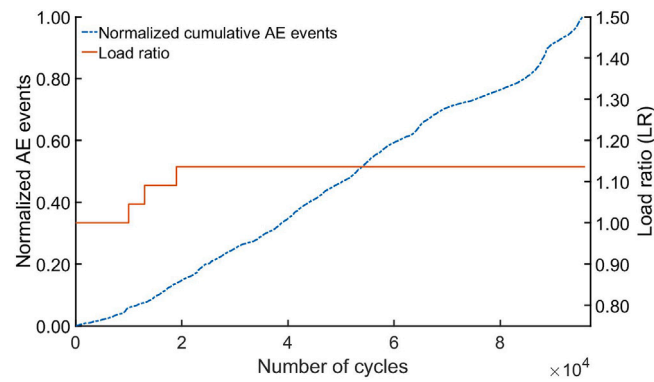


Fig. 30. As Fig. 26 but for C.3.3.

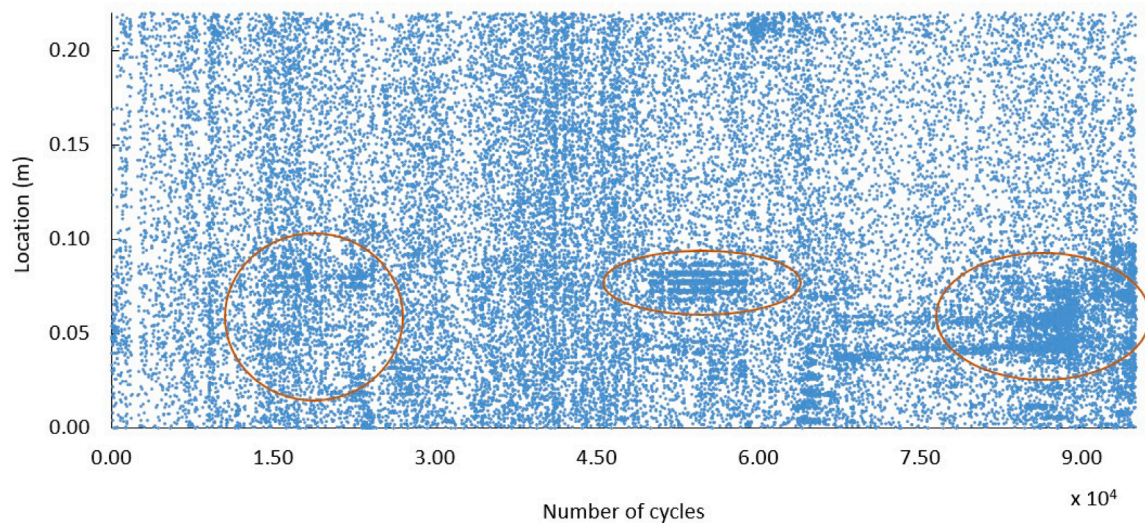


Fig. 31. As Fig. 27 but for the C.3.3.

impacts, the acoustic emission technique also showed that the fatigue damage accumulation occurred in the vicinity of the impact zone during the full fatigue test.

During the transportation and installation of a wind turbine blade damage can occur, therefore, it is important to identify the initial fatigue damage caused by impacts and monitor any further accumulation of fatigue damage. This study has shown that the spatial distribution of AE events can be useful to identify damage initiation and monitor fatigue damage accumulation. In the spatial distribution of AE events, an increase in the local density of events can be seen as a sign of damage. In addition, a persistent high density of AE events which remains high in a specific area relative to other areas indicates progressive damage in that area.

A future study should be focused on how to relate this local density of AE events to the severity of damage for which artificial intelligence techniques may be helpful. Acoustic measurements using piezoelectric transducers present practical limitations, as they are not easily implementable on wind turbine blades. The need for long-term attachment to blades, especially in harsh environmental conditions, poses significant challenges [33]. Microelectromechanical systems (MEMS) and fiber optic sensors offer easier deployment options but come with limitations in sensitivity. However, MEMS and fiber optic sensors, being thin, can be readily installed on blades, and fiber optic sensors can even be embedded inside the blade [34,35]. These types of sensors have been shown to be suitable for making ultrasonic acoustic measurements for the purposes of structural health monitoring [36,37].

It is important to note that these results were obtained under laboratory conditions. Further experimental validation with additional

data is required to assess their accuracy in real severe environmental conditions, such as during high winds, periods of rain, thunderstorms, or when significant noise is generated by turbine structures.

CRediT authorship contribution statement

S. Khoshmanesh: Writing – original draft, Visualization, Validation, Software, Resources, Project administration, Methodology, Investigation, Formal analysis, Data curation, Conceptualization. **S.J. Watson:** Conceptualization, Methodology, Supervision, Validation, Visualization, Writing – review & editing. **D. Zarouchas:** Conceptualization, Methodology, Project administration, Resources, Supervision, Validation, Visualization, Writing – review & editing.

Declaration of competing interest

The authors declare that they have no known competing financial interests or personal relationships that could have appeared to influence the work reported in this paper.

Data availability

Data will be made available on request.

Acknowledgments

All experimental tests were conducted in the structure laboratory at the Aerospace Faculty of the Delft University of Technology (TU Delft). The authors would like to thank the laboratory staff for their support during these experiments.

References

- [1] Shanker Verma A, Vedvik PN, Gao Z. A comprehensive numerical investigation of the impact behaviour of an offshore wind turbine blade due to impact loads during installation. *Ocean Eng* 2019;172:127–45. <http://dx.doi.org/10.1016/j.oceaneng.2018.11.021>.
- [2] Khoshmanesh S, Watson S, Zarouchas D. The effect of the fatigue damage accumulation process on the damping and stiffness properties of adhesively bonded composite structures. *Compos Struct* 2022.
- [3] Sørensen FB, Holmes J, Brøndsted P, Branner K. Blade materials, testing methods and structural design. *WIT Trans State-art Sci Eng* 2010;44:417–66.
- [4] Mishnaevsky L, Branner K, Petersen H, Beauson J, Mcgwan M, Sørensen FB. Materials for wind turbine blades: An overview. *Materials* 2017;10.
- [5] Chou HY, Mouritz AP, Bannister MK, Bunsell AR. Acoustic emission analysis of composite pressure vessels under constant and cyclic pressure. *Composites A* 2015;70:111–20. <http://dx.doi.org/10.1016/j.compositesa.2014.11.027>.
- [6] Lissek F, Haeger A, Knoblauch V, Hloch S, Pude F, Kaufeld M. Acoustic emission for interlaminar toughness testing of CFRP: Evaluation of the crack growth due to burst analysis. *Composites B* 2018;136:55–62. <http://dx.doi.org/10.1016/j.compositesb.2017.10.012>.
- [7] Nikbakht M, Yousefi J, Hosseini-Toudeshky H, Minak G. Delamination evaluation of composite laminates with different interface fiber orientations using acoustic emission features and micro visualization. *Composites B* 2017;113:185–96. <http://dx.doi.org/10.1016/j.compositesb.2016.11.047>.
- [8] Barile C. Innovative mechanical characterization of CFRP by using acoustic emission technique. *Eng Fract Mech* 2019;210:414–21. <http://dx.doi.org/10.1016/j.engfracmech.2018.02.024>.
- [9] Saidane EH, Scida D, Pac M-J, Ayda R. Mode-I interlaminar fracture toughness of flax, glass and hybrid flax-glass fibre woven composites: Failure mechanism evaluation using acoustic emission analysis. *Polym Test* 2019;75:246–53. <http://dx.doi.org/10.1016/j.polymertesting.2019.02.022>.
- [10] Tabrizi EI, Kefal A, Monfared Zanjani SJ, Cagdas Akalin C, Yildiz M. Experimental and numerical investigation on fracture behavior of glass/carbon fiber hybrid composites using acoustic emission method and refined zigzag theory. *Compos Struct* 2019;223. <http://dx.doi.org/10.1016/j.compstruct.2019.110971>.
- [11] Ali QH, Tabrizi EI, Awais Khan MR, Tufani A, Yildiz M. Microscopic analysis of failure in woven carbon fabric laminates coupled with digital image correlation and acoustic emission, composite structures. *Compos Struct* 2019;230. <http://dx.doi.org/10.1016/j.compstruct.2019.111515>.
- [12] Ameer BM, El Mahi A, Rebiere J-C, Gimenez I, Beyaoui M, Abdennadher M, et al. Investigation and identification of damage mechanisms of unidirectional carbon/flax hybrid composites using acoustic emission. *Eng Fract Mech* 2019;216. <http://dx.doi.org/10.1016/j.engfracmech.2019.106511>.
- [13] Haggui M, El Mahi A, Jendli Z, Akrouf A, Haddar M. Static and fatigue characterization of flax fiber reinforced thermoplastic composites by acoustic emission. *Appl Acoust* 2019;147:100–10. <http://dx.doi.org/10.1016/j.apacoust.2018.03.011>.
- [14] Khademi R, Abdi S, Ghorbani A, Ghiami A, Erden S. Damage characterization of carbon/epoxy composites using acoustic emission signals wavelet analysis. *Compos Interfaces* 2020;27(1):111–24. <http://dx.doi.org/10.1080/09276440.2019.1601939>.
- [15] Saeedifar M, Saleh NM, Teixeira De Freitas S, Zarouchas D. Damage characterization of adhesively-bonded Bi-material joints using acoustic emission. *Composites B* 2019;176. <http://dx.doi.org/10.1016/j.compositesb.2019.107356>.
- [16] Saeedifar M, Mansvelder J, Mohammadi R, Zarouchas D. Using passive and active acoustic methods for impact damage assessment of composite structures. *Compos Struct* 2019;226. <http://dx.doi.org/10.1016/j.compstruct.2019.111252>.
- [17] Pascoe JA, Zarouchas D, Alderliesten RC, Benedictus R. Using acoustic emission to understand fatigue crack growth within a single load cycle. *Eng Fract Mech* 2018;194:281–300. <http://dx.doi.org/10.1016/j.engfracmech.2018.03.012>.
- [18] Roundi W, El Mahi A, El Gharad A, Rebiere J-L. Acoustic emission monitoring of damage progression in glass/epoxy composites during static and fatigue tensile tests. *Appl Acoust* 2018;132:124–34. <http://dx.doi.org/10.1016/j.apacoust.2017.11.017>.
- [19] Saeedifar M, Ahmadi Najafabadi M, Zarouchas D, Hosseini Toudeshky H, Jalalvand M. Clustering of interlaminar and intralaminar damages in laminated composites under indentation loading using acoustic emission. *Composites B* 2018;144:206–19. <http://dx.doi.org/10.1016/j.compositesb.2018.02.028>.
- [20] Saeedifar M, Najafabadi A, M. Zarouchas D, Hosseini Toudeshky H, Jalalvand M. Barely visible impact damage assessment in laminated composites using acoustic emission. *Composites B* 2018;152:180–92. <http://dx.doi.org/10.1016/j.compositesb.2018.07.016>.
- [21] Malpot A, Touchard F, Bergamo S. An investigation of the influence of moisture on fatigue damage mechanisms in a woven glass-fibre-reinforced PA66 composite using acoustic emission and infrared thermography. *Composites B* 2017;130:11–20. <http://dx.doi.org/10.1016/j.compositesb.2017.07.017>.
- [22] Zhou W, Zhang P, Zhang Y. Acoustic emission based on cluster and sentry function to monitor tensile progressive damage of carbon fiber woven composites. *Appl Sci* 2018;8(11). URL <https://www.mdpi.com/2076-3417/8/11/2265>.
- [23] Tang J, Souza S, Mares C, Gan T. A pattern recognition approach to acoustic emission data originating from fatigue of wind turbine blades. *Sensors* 2017;17(11). URL <https://www.mdpi.com/1424-8220/17/11/2507>.
- [24] Sørensen FB, Jørgensen E, Debel PC, Jensen FM, Jensen MH, Jacobsen KT, et al. Improved design of large wind turbine blade of fibre composites based on studies of scale effects (Phase 1). *Risø National Laboratory Information Service Department*; 2004.
- [25] Sundaresan M, Schulz M, Ghoshal A. Structural health monitoring static test of a wind turbine blade: August 1999. *Nat Renew Energy Lab, NREL/SR* 2002;85. <http://dx.doi.org/10.2172/15000129>.
- [26] Mishnaevsky L. Root causes and mechanisms of failure of wind turbine blades: Overview. *Materials* 2022;15(9):2959. <http://dx.doi.org/10.3390/ma15092959>.
- [27] Shohag MA, Hammel E, Olawale D, Okoli O. Damage mitigation techniques in wind turbine blades: A review. *Wind Eng* 2017;41. <http://dx.doi.org/10.1177/0309524X17706862>.
- [28] Ciang CC, Lee J-R, Bang H-J. Structural health monitoring for a wind turbine system: A review of damage detection methods. *Meas Sci Technol* 2008;19(12):122001. <http://dx.doi.org/10.1088/0957-0233/19/12/122001>.
- [29] Zarouchas D, Maris AA, Sayer F, Van Hemelryck D, Van Wingerde AM. Investigations on the mechanical behavior of a wind rotor blade subcomponent. *Composites B* 2012;43:647–54. <http://dx.doi.org/10.1016/j.compositesb.2011.10.009>.
- [30] Sayer F, Antoniou A, Van Wingerde A. Investigation of structural bond lines in wind turbine blades by sub-component tests. *Int J Adhes Adhes* 2012;37:129–35. <http://dx.doi.org/10.1016/j.ijadhadh.2012.01.021>.
- [31] Romhany G, Czizany T, Karger-Kocsis J. Failure assessment and evaluation of damage development and crack growth in polymer composites via localization of acoustic emission events: A review. *Polym Rev* 2017;57(3):397–439. <http://dx.doi.org/10.1080/15583724.2017.1309663>.
- [32] Drouillard TF. Acoustic emission: The first half century. In: *Conference: 12. international acoustic emission symposium, Sapporo (Japan), 21 Oct 1994*. 1994, RFP-4875; CONF-9410182-1 ON: DE94017176.
- [33] Tcherniak D, Mølgaard LL. Active vibration-based structural health monitoring system for wind turbine blade: Demonstration on an operating vestas V27 wind turbine. *Struct Health Monit* 2017;16(5):536–50. <http://dx.doi.org/10.1177/1475921717722725>.
- [34] Loss T, Bergmann A. Vibration-based fingerprint algorithm for structural health monitoring of wind turbine blades. *Appl Sci* 2021;11(9):4294. <http://dx.doi.org/10.3390/app11094294>, URL <http://dx.doi.org/10.3390/app11094294>.
- [35] Cazzulani G, Cinquemani S, Benedetti L, Belloli M. Load estimation and vibration monitoring of scale model wind turbine blades through optical fiber sensors. *Eng Res Exp* 2021;3(2):025036. <http://dx.doi.org/10.1088/2631-8695/ac060e>.
- [36] Bao X. Prospects on ultrasound measurement techniques with optical fibers. *Meas Sci Technol* 2023;34(5):051001. <http://dx.doi.org/10.1088/1361-6501/acb5b2>.
- [37] Haus JN, Lang W, Roloff T, Rittmeier L, Bornemann S, Sinapius M, et al. MEMS vibrometer for structural health monitoring using guided ultrasonic waves. *Sensors* 2022;22(14). <http://dx.doi.org/10.3390/s22145368>, URL <https://www.mdpi.com/1424-8220/22/14/5368>.